

H2R: A Human-to-Robot Data Augmentation for Robot Pre-training from Videos

Guangrun Li^{1*}, Yaoxu Lyu^{1*}, Zhuoyang Liu^{1*}, Chengkai Hou^{1*†}, Jieyu Zhang², Shanghang Zhang¹ 

¹State Key Laboratory of Multimedia Information Processing, School of Computer Science, Peking University;

²University of Washington

* Equal contribution, [†] Project lead,  Corresponding author

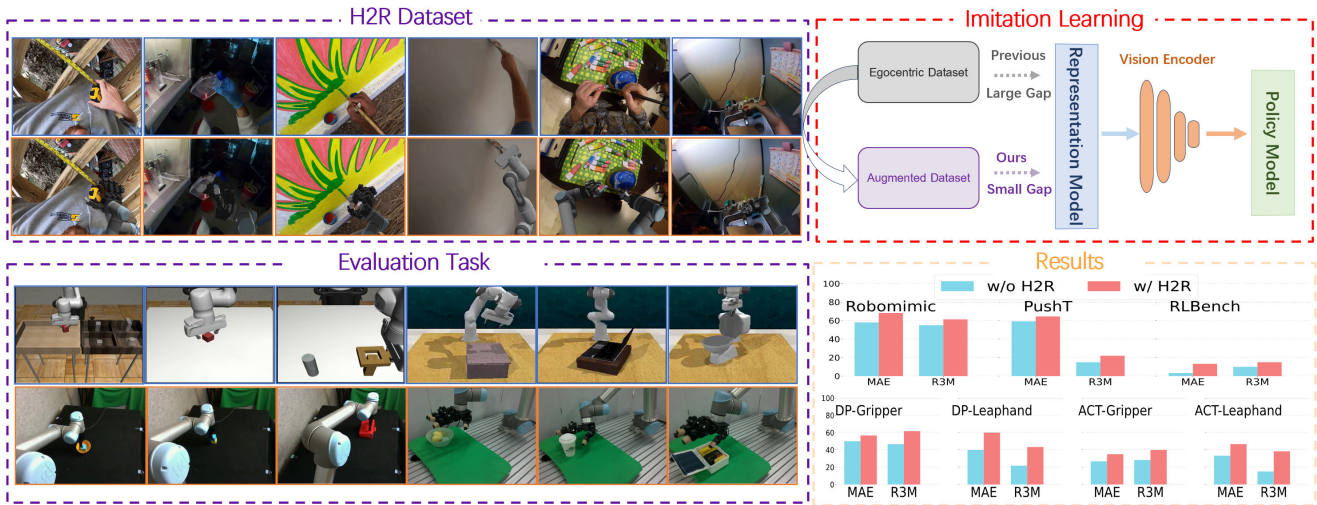


Figure 1. **Overview of H2R.** H2R is a data augmentation technique designed to enhance robot pre-training by converting first-person human hand operation videos into robot-centric visual data. By bridging the visual domain gap, H2R improves pre-trained visual encoders for downstream robot policies (imitation learning), validated across simulation benchmarks and real-world robotic tasks.

Abstract

Large-scale pre-training using videos has proven effective for robot learning. However, the models pre-trained on such data can be suboptimal for robot learning due to the significant visual gap between human hands and those of different robots. To remedy this, we propose **H2R**, a simple data augmentation technique that detects human hand keypoints, synthesizes robot motions in simulation, and composites rendered robots into egocentric videos. This process explicitly bridges the visual gap between human and robot embodiments during pre-training. We apply H2R to augment large-scale egocentric human video datasets such as Ego4D and SSv2, replacing human hands with simulated robotic arms to generate robot-centric training data. To verify the effectiveness of the augmentation pipeline, we introduce a CLIP-based image-text similarity metric that quantitatively evaluates the semantic fidelity of robot-rendered frames to

the original human actions. We validate H2R across four simulation benchmarks—Robomimic, RLBench, PushT and CortexBench, and real-world manipulation tasks with UR5 and Dual-Arm Franka/UR5. H2R consistently improves downstream success rates, yielding gains of **1.3%–10.2%** in simulation and **3.3%–23.3%** in real-world tasks across various visual encoders and policy learning methods. We further demonstrate the potential of H2R in cross-embodiment generalization and its compatibility with VLA models. These results indicate that H2R improves the generalization ability of robotic policies by mitigating the visual discrepancies between human and robot domains. The project page is available in <https://sites.google.com/view/h2r-robotics>.

1. Introduction

Pre-training of generalizable robotic features for object manipulation and motion navigation constitutes a crucial objective within the realm of robotics. Inspired by the remarkable

accomplishments of large scale pre-training in computer vision [21, 28, 36, 47, 66] and natural language processing [1, 2, 13, 42, 64], many efforts have been devoted to harnessing large-scale data to construct generalizable representations in the robotics field [5, 6, 48]. Nevertheless, when it comes to robot manipulation, the process of collecting demonstrations is labor-intensive and expensive [6, 16–18, 22, 29, 32, 35, 38, 40]; meanwhile, there exist many large-scale egocentric video datasets showing how humans perform manipulation and navigation, which can potentially serve as a cheap alternative of demonstrations for the pre-training of generalizable visual features for robotics.

Recent works [47, 62, 67] analyze such egocentric human video datasets such as Ego4D [25], SSv2 [24], and Epic Kitchens [11] with the aim of gleaning prior knowledge about object manipulation and enabling the acquisition of general and robust feature representations. However, during the representation learning, the gap in visual representations between the human arm and the robotic arm remains largely unaddressed and can hinder the transferability of models trained on egocentric datasets to robotic systems. Specifically, when utilizing the robot expert data to fine-tune the pre-trained robotic representations for downstream robotic tasks, the model has to learn to bridge the visual gap between the first-person human hand and the robots in addition to acquiring nuanced task-specific skills demonstrated in the robot expert data. This would result in increased complexity during the fine-tuning process and suboptimal performance.

To mitigate this issue, we propose H2R (as shown in Figure 1), a simple data augmentation method that converts videos of **Human** hand operations into that of **Robotic** arm manipulation. H2R consists of two major procedures: the first part is to generate the robotic movements to imitate the human hand movements in a video, followed by the second stage that overlays the robotic movements onto the human hand’s movements in the video. Specifically, in the first part, we employ state-of-the-art 3D hand reconstruction model HaMeR [50] to accurately detect the position and posture of the human hand in egocentric videos. Then, we simulate the same robot state in simulators to obtain the mask of robot actions. In the second stage, we use the Segment Anything Model [39] to automatically separate human hand from background, and use the inpainting model LaMa [60] to fill the removed hand mask. After that, we align the camera intrinsic parameters of the images detected in HaMeR with those in the simulator, and then achieve pixel-level matching between the robotic arm images in the simulators and the human hand images in the egocentric video. Finally, we overlay the robotic arm images captured by the simulator’s camera onto the areas where the human hands are removed. Through such a process, H2R explicitly reduces the gap between human and robot hands by creating realistic robotic arm movements that visually mimic human

hand actions. It allows the model to learn the task-specific actions demonstrated by the human hand, but with robotic arm visual representations that are more suitable for robotic systems.

To evaluate the effectiveness of the H2R augmentation process, we introduce a CLIP-based semantic similarity metric that measures how well the rendered robot frames preserve the original action semantics. This provides a lightweight and scalable proxy to assess the alignment quality between input human videos and robot-augmented outputs.

To further verify the utility of the augmented datasets, we conduct downstream experiments comparing models pre-trained on original egocentric datasets with those trained on our released H2R-enhanced datasets. These comparisons are performed on both simulation and real-world robotic manipulation tasks to assess how H2R impacts policy learning performance in practice. For the pre-training stage, we apply MAE [28] and R3M [47] frameworks to train visual encoders using 62,500 videos from the SSv2 dataset, where 16 keyframes are sampled per video. The pretrained visual representations are used in downstream imitation learning pipelines. We conduct comprehensive evaluations across both simulation and real-world manipulation tasks. In simulation, we evaluate pre-trained visual encoders on four benchmark suites: Robomimic, RLBench, PushT and CortexBench. H2R improves the average success rates by +10.2% for MAE and +6.3% for R3M on Robomimic tasks, +10.0% for MAE and +5.0% for R3M on RLBench tasks, +5.3% for MAE and +7.0% for R3M on the PushT task, and +5.3% for MAE and +1.3% for R3M on the CortexBench task. In real-world experiments, we deploy H2R-enhanced encoders on different robot and end-effector settings, evaluated over nine manipulation tasks under two policy frameworks: Diffusion Policy (DP) [10] and ACT [68]. H2R brings consistent improvements, with average success rate gains of +10.0% (MAE) and +14.1% (R3M) under DP, and +12.8% (MAE) and +13.3% (R3M) under ACT. H2R also improves MAE/R3M performance when pre-trained on Ego4D, with up to +10% and +15% gains in simulated and real-world tasks, respectively. Beyond these evaluations, we also test H2R’s ability to support cross-embodiment transfer by pre-training encoders on Franka data and deploying them on UR robots, indicating that H2R improves representation transfer across different morphologies. In addition, fine-tuning VLA backbones on H2R-generated datasets yields markedly higher success rates on dual-arm UR tasks than fine-tuning on human-hand videos or using no fine-tuning. These results demonstrate that H2R effectively bridges the human-to-robot visual domain gap and significantly enhances downstream performance across both simulation and real-world manipulation settings.

2. Related Work

Robot Imitation Learning. Data-driven policy learning [10, 41, 45, 48, 62, 63] has enabled robots to autonomously perform tasks such as grasping, locomotion, and manipulation. Imitation learning [10, 46, 65, 68] trains policies from successful demonstrations, often supervised by behavior cloning [19, 61] objectives. ACT [68] addresses non-Markovian dynamics by fusing temporal sequences, while diffusion models [10, 65] are introduced to handle the inherent multimodality of robot motions. In addition, CordViP [20] leverages 3D object-robot correspondences to enhance dexterous manipulation.

Visual Encoder Pretraining for Robotics. Visual pretraining improves generalization of robotic policies across diverse tasks. Researchers have explored architectural designs [14, 26], training objectives [8, 9, 27], and dataset compositions [12, 44, 56, 57]. PVR-Control [49] shows that pretrained visual representations can outperform direct state-based policies. RPT [54] tokenizes observations to enable masked prediction pretraining. Methods like MVP [52] and R3M [47] utilize self-supervised objectives on videos to learn representations transferable to reinforcement learning. Voltron [36] demonstrates the use of MAE and contrastive learning for hierarchical robot control.

Cross-Domain Visual Alignment. Bridging the domain gap between human and robot visual inputs remains a major challenge. WHIRL [3] matches task structure from third-person views, while RoVi-Aug [7] and Mirage [53] manipulate appearance via segmentation or image-space preprocessing. EgoMimic [37] removes hands and normalizes views to align egocentric perspectives.

3. H2R: Human-to-Robot Data Augmentation

In this section, we describe **H2R**, a data augmentation pipeline for robot learning from egocentric human videos (Figure 2). It replaces human hands in every frame with robotic arms equipped with various end effectors, generating a new, visually different dataset. This approach aims to mitigate the visual gap between human hands and robots, thereby improving the generalizability of visual representations learned from egocentric data to robotic domains. We first examine the position and pose of the hand and arm in the image, then map this pose to the robotic arm and end-effector in the simulator. Next, we erase the original hand and arm from the image and overlay a rendered image of the simulated robot performing the same pose onto the original image in place of the removed hand and arm. Figure 4 illustrates examples of human hand videos that have been processed using H2R.

3.1. H2R Data Augmentation Pipeline

3D Hand Pose Estimation. In order to overlay the human hands in the egocentric image with different robots, we first need an efficient and accurate model to detect hand information. We adopt HaMeR [50], a state-of-the-art model for 3D hand detection and reconstruction, to accurately locate the hand in the image, providing precise positional information for subsequent hand removal. Given an ego-centric RGB image, HaMeR estimates both the hand pose (including 3D keypoints) and the intrinsic and extrinsic parameters of the rendering camera.

Robotic Arm and End Effector Construction. This step involves building the robotic arm and its end-effectors, which are typically either grippers or dexterous hands. For dexterous hands, we estimate joint angles from hand keypoints predicted by HaMeR. Each finger joint angle is calculated using three consecutive keypoints along that finger. For grippers, we determine how open or closed they are based on the Euclidean distance between the corresponding fingertips. Since hand keypoints don't capture the full arm pose (especially for joints unrelated to the hand), we manually set reasonable values for the remaining arm joints to complete a plausible robot configuration.

Simulator Camera Position Alignment. The visual bias introduced by the camera perspective is more significant than the action retargeting itself. To address this, we use the hand keypoints and camera parameters from HaMeR to adjust the camera pose in the simulator. Specifically, we define two coordinate systems: C_H , the coordinate system aligned with the human hand, and C_S , the coordinate system of the robotic arm in the simulator. By mapping the position of the camera in C_H to C_S , we can ensure that the camera in the simulator shares the same perspective as the one captured in the real-world egocentric human image. The original camera position ${}^W \mathbf{cam}_{real}$ in the world frame is transformed to the aligned simulator position ${}^W \mathbf{cam}_{sim}$ using transformations from human hand (${}_H^W \mathbf{R}$) and robot simulator (${}_S^W \mathbf{R}$) coordinate systems:

$${}^W \mathbf{cam}_{sim} = {}_S^W \mathbf{R} \times {}_H^W \mathbf{R}^{-1} \times {}^W \mathbf{cam}_{Real} \quad (1)$$

A more detailed explanation of the coordinate transformation and camera alignment process is provided in Appendix.

Robot Hand Rendering and Copy-paste. After setting the camera, the segmentation mask of the robotic arm is obtained by rendering with the simulator camera. We directly obtain the pixel coordinates of the human hand keypoints from HaMeR, which are predicted from the input image. In parallel, the pixel coordinates of the robot end-effector links are computed in the simulator by projecting their 3D positions through the aligned camera using the known transformation matrices. By aligning the robot link positions with the corresponding human hand keypoints in pixel space, we ensure that the overlaid robot hand accurately matches the

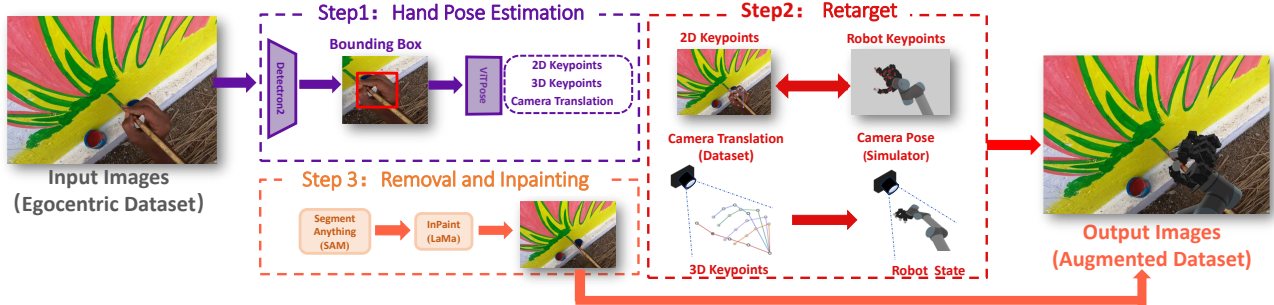


Figure 2. **H2R Pipeline.** H2R involves replacing human hands with robotic arms by first using the HaMeR model to detect hand poses and camera parameters. The human hand is then removed using the SAM, and the inpainting model LaMa fills in the gap. A robot hand is constructed based on the detected pose and keypoints, with the camera perspective adjusted to match the original image. Finally, the robot hand is overlaid onto the image, ensuring accurate alignment with the human hand.

position and orientation of the original hand in the image, achieving precise pixel-level alignment.

Human Arm and Hand Removal. After obtaining the hand pose information, we need to mask out the human hand and then inpaint the masked area with a proper background. We use Segment Anything Model (SAM) [39] to automatically segment the human hand and arm regions using the hand pose information detected by HaMeR. Then, to obtain clean backgrounds for inserting robotic arms, we apply LaMa [60], a powerful inpainting model, to fill in the removed hand-arm region. This yields clean RGB images without human limbs, providing a seamless background for inserting robotic arms in the subsequent steps.

3.2. Data Quality Evaluation



Figure 3. **H2R samples.** Visual comparison between original human data (top) and our augmented data (bottom).

To assess the visual plausibility and semantic consistency of the robot-augmented images produced by H2R, we employ a vision-language similarity evaluation based on CLIP [51]. This method measures how well the rendered robot actions align with high-level semantic descriptions of manipulation tasks. For each augmented frame, we formulate a pair of textual prompts describing the same action: one from a human-centric perspective and one from a robot-centric perspective. The human-centric template is defined as: A human is *[action]*; the robot-centric template is defined as: A robotic arm is *[action]*. Here, *[action]* is a natural language phrase describing the high-level behavior, such as "holding a bottle" or "brushing paint on a wall".

We use the CLIP ViT-B/32 model to compute the cosine similarity between the image embedding of the augmented frame and the corresponding textual prompt. This yields

a scalar score reflecting how semantically consistent the image content is with the robot-centric description. Similarly, we compute the similarity between the original human frame and the human-centric prompt. This setup allows us to directly compare semantic alignment before and after augmentation under their respective modalities. For each frame, only the action-relevant region is retained, and background context is preserved via inpainting using LaMa. We average similarity scores over multiple samples per action class to mitigate variance and isolate the impact of robotic replacement. All textual prompts are manually curated to maintain consistency across frames and embodiments.

Figure 3 contains six pairs of subfigures, each showing a human action and its corresponding augmented robotic action. The six action pairs in Figure 3 (left to right) are described as follows: (1) Holding a yellow measuring tape at a construction site; (2) Holding a bottle; (3) Painting on the wall with a brush; (4) Rushing paint on a wall; (5) Turning on the kitchen faucet; (6) Preparing painting materials on a table.

The CLIP similarity scores are reported in Table 1. Across all samples, H2R-augmented images consistently achieve higher similarity with robot-centric action descriptions than original images do with human-centric ones. This confirms that H2R augmentation effectively improves visual-semantic alignment between human demonstrations and robotic execution. This evaluation provides a lightweight, scalable, and

Table 1. **CLIP similarity scores.** Higher values indicate better alignment between images and action descriptions.

	Img-1	Img-2	Img-3	Img-4	Img-5	Img-6
Ori	30.6	23.7	31.2	31.7	27.5	28.7
Aug	32.6	28.9	32.3	32.0	28.7	31.0

interpretable metric for assessing how well visual hand-to-robot transformations preserve task semantics. To quantify data quality, we sample 1,000 image pairs (original and H2R-augmented). For each original image, we use Qwen-



Figure 4. **Examples of H2R Augmentation.** Each column shows images before and after augmentation. The top row uses UR5 Leaphand, the middle row uses UR5 Gripper, and the bottom row uses Franka to replace human hands.

2.5-VL [4] to generate a verb-noun action description (e.g., “washing bowl”). We then form two prompts: “A human is [action]” and “A robot arm is [action]”. Using CLIP ViT-B/32, we compute the cosine similarity between: (1) the human prompt and the original image, and (2) the robot prompt and the H2R-augmented image. We report the average similarity over all 1,000 samples. The raw images achieve an average score of 28.01, while H2R-augmented images reach 29.83. This demonstrates that H2R-augmented images exhibit stronger semantic alignment with robot-centric action descriptions, confirming improved visual-semantic coherence for robotic manipulation. The results validate our data curation pipeline as effective for generating high-quality, robot-relevant visual data at scale.

4. Simulation Experiment

Encoder Pre-training. We adopt the MAE [28, 62] and R3M [47] frameworks for pre-training, each employing a Vision Transformer (ViT) Base [15] model as the visual encoder. The training dataset used is a subset of **Ego4D** (117K clips) or **SSv2** (1M images). Both MAE and R3M are pre-trained with $8 \times$ A800 GPUs. MAE employs 800 epochs with 128 batch size and 4e-4 learning rate, while R3M uses 20K steps with 256 batch size and 1e-4 learning rate.

Policy Training. We train for 200 steps and report the mean success rate for Robomimic tasks. For tasks in RL-Bench [31], we train for 800 epochs for each policy model and test them 20 times in the RL-Bench environment with a random initialization. For the PushT task, we train the Diffusion Policy model for 200 epochs and report the success rate in the simulation environment. For VC-1 Cortex benchmark, we train policies using behavior cloning composed of

a 3-layer MLP for 100 epochs. The training hyperparameters used in this work are identical to those described in the original paper.

Simulation Benchmark. For each pre-training method, we evaluate the performance of pre-trained encoders in imitation learning. Specifically, we select a total of seven simulation tasks in different environments, which are from Robomimic [46], RLbench [31], and Diffusion Policy [10]. In particular, for Robomimic, we train the policies using the behavior cloning (BC) and evaluate them on tasks such as **MoveCan**, **Square**, and **Lift**, where the robot performs actions such as moving or lifting objects. For RLBench, we train the policies with Diffusion Policy and evaluate them on three manipulation tasks: **Close Box**, **Close Laptop Lid** and **Toilet Seat Down**. We use the **PushT** task in the Diffusion Policy evaluation framework, which evaluates a robot’s ability to push an object to a target location. We also use three MetaWorld tasks: **Assembly**, **ButtonPress** and **Hammer** from VC-1 Cortex benchmark for evaluation. An overview of these simulation tasks is shown in Appendix.

4.1. Simulation Results

Table 2 shows encoders trained on augmented data **H2R-SSv2** significantly outperform those on original **SSv2** across all simulation tasks. For Robomimic tasks, MAE achieves a 10.2% average success rate improvement and R3M 6.3%, with MAE seeing a substantial **25.5%** gain on MoveCan. On PushT, H2R boosts MAE by **5.3%** and R3M by **7.0%**. In RLBench, MAE improves its performance by **10.0%** on average and R3M by **5.0%**. In CortexBench, H2R improves MAE by **5.3%** and R3M by **1.3%**. These results confirm that the H2R-augmented dataset delivers superior visual representations for imitation learning to those learned from large-scale human video datasets like **SSv2**, as H2R bridges the visual gap between human hands and robotic arms to enhance vision encoder pre-training performance.

In addition to **SSv2** dataset, we also perform the same experiments on the PushT task and the tasks in RLbench benchmark using the **Ego4D** dataset. The experimental results in the simulator are shown in Table 3, which indicates that H2R remains highly effective when applied to the Ego4D dataset.

4.2. Pretraining Model on Robotic Datasets

To further evaluate how H2R compares to models pretrained directly on robotic datasets, we refer to a recent study [34], which conducted a systematic comparison between visual representations pretrained on large-scale egocentric human video datasets and those trained on robotic datasets such as DROID [38]. The experimental results, summarized in Table 4, show that models pretrained on robotic datasets often provide limited or even degraded performance on downstream manipulation Robomimic benchmarks. Moreover, despite being smaller and simulated rather than real-robot

Table 2. Simulation Benchmark Results. Success rates (%) across imitation learning tasks in Robomimic, PushT, RLBench and CortexBench, evaluated with MAE and R3M encoders before and after applying H2R. **Blue** represents an increase in task success rate, while **Red** represents a decrease. All subsequent tables follow the same rule.

	Robomimic				Diffusion Policy				RLBench				CortexBench				
	MoveCan	Square	Lift	Average	PushT	CloseBox	CloseLaptopLid	ToiletSeatDown	Average	Assembly	ButtonPress	Hammer	Average	Assembly	ButtonPress	Hammer	Average
MAE (SSv2)	54.0	25.5	94.5	58.0	59.2	0.0	10.0	0.0	3.3	84.0	80.0	96.0	86.7				
MAE (H2R-SSv2)	79.5 (+25.5%)	29.5 (+4.0%)	95.5 (+1.0%)	68.2 (+10.2%)	64.5 (+5.3%)	5.0 (+5.0%)	15.0 (+5.0%)	20.0 (+20.0%)	13.3 (+10.0%)	88.0 (+4.0%)	88.0 (+8.0%)	100.0 (+4.0%)	92.0 (+5.3%)				
R3M (SSv2)	59.5	20.5	85	55	15	0	20	10	10	76.0	56.0	88	73.3				
R3M (H2R-SSv2)	61.5 (+2.0%)	37.5 (+17.0%)	85.0 (0.0%)	61.3 (+6.3%)	22.0 (+7.0%)	5.0 (+5.0%)	20.0 (0.0%)	20.0 (+10.0%)	15.0 (+5.0%)	68.0 (-8.0%)	60.0 (+4.0%)	96.0 (+8.0%)	74.7 (+1.3%)				

Table 3. Results on Ego4D Dataset. Success rates (%) across imitation learning tasks in the PushT and RLBench environments.

	RLBench				
	PushT	CloseBox	CloseLaptopLid	ToiletSeatDown	Average
MAE (Ego4D)	51.3	0	0	5	1.7
MAE (H2R-Ego4D)	53.5 (+2.2%)	10 (+10%)	5 (+5.0%)	0 (-5.0%)	5 (+3.3%)
R3M (Ego4D)	13.6	10	5	5	6.7
R3M (H2R-Ego4D)	13.6 (0.0%)	15 (+5.0%)	5 (0.0%)	15.0 (+10.0%)	11.7 (+10.0%)

Table 4. Comparison with model pretrained on robotic datasets. All visual encoder weights are initialized using the R3M pretraining method, with the “R3M-H2R” variant pretrained on the H2R-augmented SSv2 dataset.

	Robomimic			
	MoveCan	Square	Lift	Average
R3M	59.5	20.5	85.0	55.0
R3M-H2R	61.5	37.5	85.0	61.3
R3M-DROID	54.0	22.0	96.0	56.7

data, the H2R dataset outperforms the DROID dataset in pre-training effectiveness, indicating its strong potential for robotic model pre-training and reflecting its high data quality.

4.3. Effects of Demonstration Density

The relatively low success rates observed in Table 2 are primarily due to our use of keypoint frames in RLBench tasks. This approach, widely adopted in the RLBench benchmark [23, 33, 59], accelerates both training and evaluation by reducing redundant frames. However, selecting only keyframes inevitably decreases the density of demonstration data. Since the diffusion policy employed in our imitation learning framework benefits from dense and temporally continuous data due to its long observation horizon, sparse sampling may limit its performance.

To further investigate demonstration density impact and validate H2R’s robustness, we retrain the diffusion policy with a dense RLBench dataset under identical settings. Table 5 shows higher data density significantly boosts overall success rate (e.g., MAE average from 3.3% to 45.0%). Critically, H2R consistently enhances performance across sparse and dense data regimes, confirming its general effectiveness regardless of demonstration density.

5. Real World Experiment

Robot Setups. We evaluate the effectiveness of H2R across three real-world manipulation setups: (i) a UR5

Table 5. Effects of Demonstration Density. Success rates (%) across imitation learning tasks in the RLBench environments with sparse data and dense data.

Data	Model	RLBench			
		CloseBox	CloseLaptopLid	ToiletSeatDown	Average
Sparse data	MAE MAE+H2R	0.0 5.0 (+5.0%)	10.0 15.0 (+5.0%)	0.0 20.0 (+20.0%)	3.3 13.3 (+10.0%)
Dense data	MAE MAE+H2R	50.0 60.0 (+10.0%)	40.0 45.0 (+5.0%)	45.0 60.0 (+15.0%)	45.0 55.0 (+10.0%)

arm equipped with a Robotiq Gripper [55], (ii) a UR5 arm equipped with a Leaphand end effector [58], and (iii) a dual-arm Franka Emika system using parallel Grippers. Realsense [30] is mounted on the side of the robotic arm, which provides a similar viewpoint to the ego-centric human video data used in the pre-trained visual model. We provide the visualization of the robot setup in real-world scenarios in the supplementary materials.

Real-world Tasks. We set up nine tasks for gripper manipulation, dexterous manipulation and dual-arm manipulation (Figure 5). For the Gripper tasks, we design: (1) **Gripper-PickCube**, where the Gripper picks up a cube and places it into a bowl; (2) **Gripper-Stack**, where a blue cube is stacked atop a yellow cube; and (3) **Gripper-CloseBox**, where a cube is retrieved from a box, placed into a bowl, and the box lid is subsequently closed. For the Leaphand tasks, we design: (4) **Leaphand-GraspChicken**, where a toy chicken is grasped and placed into a bowl; (5) **Leaphand-StandCup**, where a fallen cup is stood upright on the table; and (6) **Leaphand-OpenBox**, where an articulated box lid is opened. For the dual-arm manipulation tasks, we design: (7) **Dualarm-PlaceToy**, where the left arm takes a toy from the pink box and the right arm moves it to the blue box; (8) **Dualarm-SweepRubbish**, where the left arm sweeps the trash into the dustpan held by the right arm; and (9) **Dualarm-WeightSauce**, where the left arm places the cup on the scale and the right arm picks up the bottle for a pouring motion. We adopt varying numbers of demonstrations, episode lengths per demonstration, and maximum action steps during evaluation for each task, as in Table 8.

Policy Training. For policy training, we select the Diffusion Policy (DP) [10] and ACT [68] as policy frameworks. We apply the pre-trained MAE and R3M visual encoders to downstream policy learning, following the same pretraining configuration described in Section 4.

Evaluation. To ensure that the initial conditions are consis-

Table 6. **Real-world Task Results.** We report the success rate (%) over real-world tasks for MAE and R3M.

Policy	Task	MAE (SSv2)	MAE (H2R-SSv2)	R3M (SSv2)	R3M (H2R-SSv2)	Policy	Task	MAE (SSv2)	MAE (H2R-SSv2)	R3M (SSv2)	R3M (H2R-SSv2)
DP	Gripper-PickCube	45	65 (+20%)	40	50 (+10%)	ACT	Gripper-PickCube	25	30 (+5%)	25	30 (+5%)
	Gripper-Stack	50	55 (+5%)	55	70 (+15%)		Gripper-Stack	20	35 (+15%)	20	40 (+20%)
	Gripper-CloseBox	55	50 (-5%)	45	65 (+20%)		Gripper-CloseBox	35	40 (+5%)	40	50 (+10%)
	Average	50	56.7 (+6.7%)	46.7	61.7 (+15%)		Average	26.7	35 (+8.3%)	28.3	40 (+11.7%)
	Leaphand-GraspChicken	40	55 (+15%)	10	35 (+25%)		Leaphand-GraspChicken	45	50 (+5%)	10	35 (+25%)
	Leaphand-StandCup	35	60 (+25%)	20	50 (+30%)		Leaphand-StandCup	25	50 (+25%)	20	60 (+40%)
	Leaphand-OpenBox	45	65 (+20%)	40	45 (+5%)		Leaphand-OpenBox	30	40 (+10%)	15	20 (+5%)
	Average	40	60 (+20%)	23.3	43.3 (+20.0%)		Average	33.3	46.7 (+13.3%)	15	38.3 (+23.3%)
	Franka-PlaceToy	10	15 (+5%)	10	25 (+15%)		Franka-PlaceToy	25	40 (+15%)	20	30 (+10%)
	Franka-SweepRubbish	15	15 (0%)	20	20 (0%)		Franka-SweepRubbish	20	35 (+15%)	20	20 (0%)
	Franka-WeightSauce	40	45 (+5%)	20	30 (+10%)		Franka-WeightSauce	30	35 (+25%)	20	25 (+5%)
	Average	21.7	25 (+3.3%)	17.7	25 (+7.3%)		Average	25	36.7 (+16.7%)	20	25 (+5%)

Table 7. **Real-world Success Rates with H2R.** We report the task success rates (%) using two robot embodiments (UR5, Franka) for data augmentation during pre-training. All models are evaluated on downstream tasks using the Leaphand end-effector, under MAE and R3M encoders with DP and ACT policies. Despite embodiment mismatch, H2R provides consistent gains over the baseline without augmentation.

Policy	Task	MAE (SSv2)	MAE (H2R-UR5-SSv2)	MAE (H2R-Franka-SSv2)	R3M(SSv2)	R3M (H2R-UR5-SSv2)	R3M (H2R-Franka-SSv2)
DP	Leaphand-GraspChicken	40	55 (+15%)	35 (-5%)	10	35 (+25%)	20 (+10%)
	Leaphand-StandCup	35	60 (+25%)	50 (+15%)	20	50 (+30%)	30 (+10%)
	Leaphand-OpenBox	45	65 (+20%)	45	40	45 (+5%)	45 (+5%)
	Average	40	60 (+20%)	43.3 (+3.3%)	21.7	43.3 (+21.7%)	31.7 (+10%)
ACT	Leaphand-GraspChicken	45	50 (+5%)	50 (+5%)	10	35 (+25%)	40 (+30%)
	Leaphand-StandCup	25	50 (+25%)	50 (+25%)	20	60 (+40%)	25 (+5%)
	Leaphand-OpenBox	30	40 (+10%)	30	15	20 (+5%)	5 (-10%)
	Average	33.3	46.7 (+13.3%)	43.3 (+10%)	15	38.3 (+23.3%)	23.3 (+8.3%)

Table 8. **Task-specific Data Collection and Evaluation Settings.**

Task	Episode Length	Num Demos	Max Steps
Gripper-PickCube	45	30	80
Gripper-Stack	43	30	80
Gripper-CloseBox	68	30	120
Leaphand-GraspChicken	150	50	500
Leaphand-StandCup	150	50	500
Leaphand-OpenBox	200	50	800
Dualarm-PlaceToy	1000	300	1500
Dualarm-SweepRubbish	1000	300	1500
Dualarm-WeightSauce	1000	300	1500

Table 9. **Ablation Study.** Ablation by removing robot overlay (**w/o Overlay**) and camera-hand retargeting (**w/o Retarget**).

Policy	Task	H2R	H2R w/o Overlay	H2R w/o Retarget
DP	Leaphand-GraspChicken	55	30 (-25%)	30 (-25%)
	Leaphand-StandCup	60	40 (-20%)	55 (-5%)
	Leaphand-OpenBox	65	20 (-45%)	45 (-20%)
	Average	60	30 (-30%)	43.3 (-16.7%)
ACT	Leaphand-GraspChicken	50	25 (-25%)	45 (-5%)
	Leaphand-StandCup	50	35 (-15%)	30 (-20%)
	Leaphand-OpenBox	40	25 (-15%)	15 (-25%)
	Average	46.7	28.3 (-18.3%)	30 (-16.7%)

tent throughout the evaluation, we randomly place the target objects within a predefined area following a uniform distribution during expert demonstrations. During the evaluation, each real-world task is rolled out **20** times. We report the success rates of these tasks to assess model quality.

5.1. Real-world Results

In the real-world tasks, we employ diffusion policy (DP) [10] and ACT [68] to drive robots in performing manipulation tasks, where the visual encoders are pre-trained using MAE

and R3M. To evaluate the effectiveness and generalization of H2R, we first conduct experiments to validate its performance enhancement when the pre-training and policy training embodiments are the same. We then perform cross-embodiment experiments to investigate the transfer effects of H2R when the pre-training and policy training embodiments differ. We finally apply H2R to fine-tune a pre-trained vision backbone in a Vision-Language-Action model, showcasing its promising potential in this advanced setting.

For identical embodiment experiment, we use UR5 or Franka robot for augmentation during pre-training, which matches the embodiment used in policy training and evaluation. As shown in Table 6, H2R provides consistent improvements across both MAE and R3M encoders for both DP and ACT policies. For Leaphand tasks under DP, H2R leads to an average improvement of **20%** (MAE) and **21.7%** (R3M). For Gripper tasks, improvements reach **6.7%** (MAE) and **15%** (R3M). For Dual-arm Franka tasks, the improvements reach **3.3%** (MAE) and **7.3%** (R3M). Similar trends are observed in ACT, with Leaphand performance increasing by **13.3%** (MAE) and **23.3%** (R3M), Gripper tasks improving by **8.3%** (MAE) and **11.7%** (R3M), and Dual-arm Franka tasks improving by **16.7%** (MAE) and **5%** (R3M).

To evaluate cross-embodiment generalization, we use Franka-augmented the SSv2 dataset with H2R pipeline. Downstream policy training and evaluation are conducted with UR5 Leaphand. As shown in Table 7, H2R still outperforms raw Ego4D despite the embodiment mismatch. Under DP, MAE improves from **40%** to **43.3%**, and R3M from **21.7%** to **31.7%**. Under ACT, MAE increases from **33.3%** to **43.3%**, and R3M from **15%** to **23.3%**.

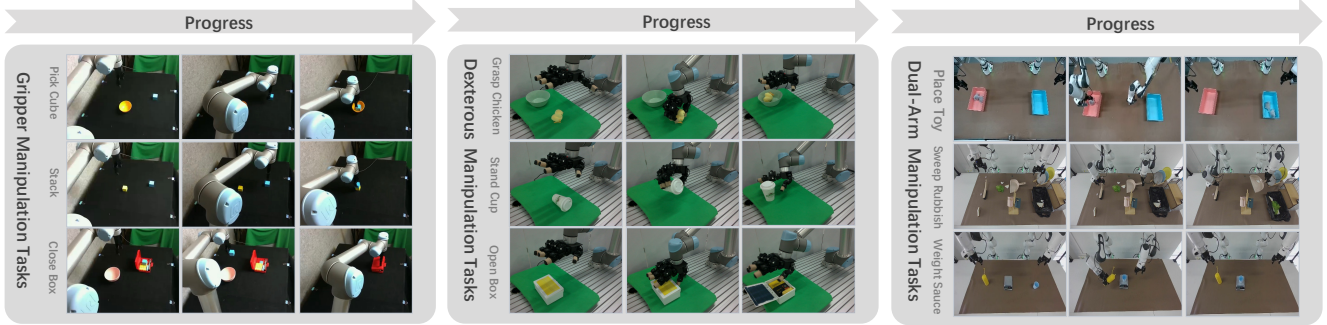


Figure 5. **Visualization of Real-world Manipulation Tasks.** The left columns show Gripper tasks and the right columns show Leaphand tasks. Each task is illustrated with three frames, demonstrating the progression from the initial state to the completion of the manipulation.

5.2. Performance on Other Datasets

Table 10. **Real-world Success Rates with Ego4D Pre-training.** We report success rates (%) on real-world Leaphand tasks using visual encoders pre-trained on the Ego4D dataset. All downstream policies are trained using ACT.

Task	MAE (Ego4D)	MAE (H2R-Ego4D)	R3M (Ego4D)	R3M (H2R-Ego4D)
Leaphand-GraspChicken	25	35 (+10%)	15	20 (+5%)
Leaphand-StandCup	25	50 (+25%)	20	25 (+5%)
Leaphand-OpenBox	35	45 (+10%)	30	40 (+10%)
Average	28.3	43.3 (+15%)	21.7	28.3 (+6.7%)

We compare encoders pre-trained on the original **Ego4D** dataset and on the H2R-augmented dataset, and apply them to real-world Leaphand manipulation tasks using the ACT [68] policy. As shown in Table 10, models trained with H2R data consistently outperform those using raw Ego4D across all three Leaphand manipulation tasks, achieving an average improvement of **15%** for MAE and **6.7%** for R3M. These results complement our findings on SSv2 and reinforce that robot-centric augmentation improves downstream real-world performance.

5.3. Potential for VLA Model Pretraining



Figure 6. **Dual-UR5 tasks.** The left columns shows PlaceBowl task and the right columns shows StackBlocks task.

A common paradigm in Vision-Language-Action (VLA) models is to initialize the visual backbone using encoders pre-trained on large-scale datasets (e.g., CLIP, VAEs). In this experiment, we investigate whether fine-tuning a pre-trained visual backbone on robot-oriented video data can enhance its suitability for robotic policy learning. Specifically, we fine-tune the pre-trained VAE encoder and decoder used in the Unified Video Action Model(UVA) [43] separately on both the original SSv2 and the H2R-augmented datasets. The fine-tuned VAEs are subsequently frozen and integrated into the UVA framework for policy training on two distinct dual-arm UR5 robot tasks(shown in Figure 6). The results

shown in Table 11 demonstrate a clear performance trend in the different variants of the UVA model.

Table 11. **Success rates of UVA variants with different visual backbones.**

Model	PlaceBowl	StackBlocks	Average
UVA	0.2	0.2	0.2
UVA + SSv2	0.1	0.2	0.15
UVA + SSv2 + H2R	0.4	0.3	0.35

5.4. Ablation Study

To evaluate the effectiveness of each component in H2R, we conduct ablation studies on two time-consuming steps: (1) performing hand inpainting without overlaying a robotic arm (H2R w/o Overlay), and (2) overlaying the arm without precise alignment between the hand and the camera, instead using random pasting (H2R w/o Retarget). Table 9 shows the necessity and effectiveness of each component in H2R. The first step leads to a significant drop in success rate due to the loss of critical human-object interaction pixels after inpainting. The second step fails to provide accurate motion cues for the model and introduces visual mismatches with real-world manipulation tasks.

6. Conclusion

We propose H2R, a data augmentation technique that bridges the visual gap between human hand demonstrations and robotic arm manipulations by replacing human hands in first-person videos with robotic arm movements. Using 3D hand reconstruction and image inpainting models, H2R generates synthetic robotic arm manipulation sequences, making them more suitable for robot pre-training. Experiments across simulation benchmarks and real-world tasks demonstrate consistent improvements in success rates for encoders trained with various pre-training methods (e.g., MAE, R3M), highlighting the effectiveness and generalization of H2R. H2R enables efficient transfer of task knowledge from human demonstrations to robotic systems, reducing the reliance on costly robot-specific data collection.

References

[1] Josh Achiam, Steven Adler, Sandhini Agarwal, Lama Ahmad, Ilge Akkaya, Florencia Leoni Aleman, Diogo Almeida, Janko Altenschmidt, Sam Altman, Shyamal Anadkat, et al. Gpt-4 technical report. *arXiv preprint arXiv:2303.08774*, 2023. 2

[2] Rohan Anil, Andrew M Dai, Orhan Firat, Melvin Johnson, Dmitry Lepikhin, Alexandre Passos, Siamak Shakeri, Emanuel Taropa, Paige Bailey, Zhifeng Chen, et al. Palm 2 technical report. *arXiv preprint arXiv:2305.10403*, 2023. 2

[3] Shikhar Bahl, Abhinav Gupta, and Deepak Pathak. Human-to-robot imitation in the wild, 2022. 3

[4] Shuai Bai, Keqin Chen, Xuejing Liu, Jialin Wang, Wenbin Ge, Sibo Song, Kai Dang, Peng Wang, Shijie Wang, Jun Tang, Humen Zhong, Yuanzhi Zhu, Mingkun Yang, Zhaohai Li, Jianqiang Wan, Pengfei Wang, Wei Ding, Zheren Fu, Yiheng Xu, Jiabo Ye, Xi Zhang, Tianbao Xie, Zesen Cheng, Hang Zhang, Zhibo Yang, Haiyang Xu, and Junyang Lin. Qwen2.5-vl technical report, 2025. 5

[5] Anthony Brohan, Noah Brown, Justice Carbajal, Yevgen Chebotar, Xi Chen, Krzysztof Choromanski, Tianli Ding, Danny Driess, Avinava Dubey, Chelsea Finn, et al. Rt-2: Vision-language-action models transfer web knowledge to robotic control, 2023. 2

[6] Anthony Brohan, Noah Brown, Justice Carbajal, Yevgen Chebotar, Joseph Dabis, Chelsea Finn, Keerthana Gopalakrishnan, Karol Hausman, Alex Herzog, Jasmine Hsu, et al. Rt-1: Robotics transformer for real-world control at scale, 2023. 2

[7] Lawrence Yunliang Chen, Chenfeng Xu, Karthik Dharmajan, Muhammad Zubair Irshad, Richard Cheng, Kurt Keutzer, Masayoshi Tomizuka, Quan Vuong, and Ken Goldberg. Rovi-aug: Robot and viewpoint augmentation for cross-embodiment robot learning, 2024. 3

[8] Ting Chen, Simon Kornblith, Mohammad Norouzi, and Geoffrey Hinton. A simple framework for contrastive learning of visual representations. *arXiv preprint arXiv:2002.05709*, 2020. 3

[9] Ting Chen, Simon Kornblith, Kevin Swersky, Mohammad Norouzi, and Geoffrey Hinton. Big self-supervised models are strong semi-supervised learners. *arXiv preprint arXiv:2006.10029*, 2020. 3

[10] Cheng Chi, Siyuan Feng, Yilun Du, Zhenjia Xu, Eric Cousineau, Benjamin Burchfiel, and Shuran Song. Diffusion policy: Visuomotor policy learning via action diffusion. *arXiv preprint arXiv:2303.04137*, 2023. 2, 3, 5, 6, 7

[11] Dima Damen, Hazel Doughty, Giovanni Maria Farinella, Sanja Fidler, Antonino Furnari, Evangelos Kazakos, Davide Moltisanti, Jonathan Munro, Toby Perrett, Will Price, et al. Scaling egocentric vision: The epic-kitchens dataset. In *Proceedings of the European conference on computer vision (ECCV)*, pages 720–736, 2018. 2

[12] Jia Deng, Wei Dong, Richard Socher, Li-Jia Li, Kai Li, and Li Fei-Fei. Imagenet: A large-scale hierarchical image database. In *2009 IEEE conference on computer vision and pattern recognition*, pages 248–255. Ieee, 2009. 3

[13] Jacob Devlin, Ming-Wei Chang, Kenton Lee, and Kristina Toutanova. Bert: Pre-training of deep bidirectional transformers for language understanding. *arXiv preprint arXiv:1810.04805*, 2018. 2

[14] Alexey Dosovitskiy, Lucas Beyer, Alexander Kolesnikov, Dirk Weissenborn, Xiaohua Zhai, Thomas Unterthiner, Mostafa Dehghani, Matthias Minderer, Georg Heigold, Sylvain Gelly, Jakob Uszkoreit, and Neil Houlsby. An image is worth 16x16 words: Transformers for image recognition at scale. In *9th International Conference on Learning Representations, ICLR 2021, Virtual Event, Austria, May 3-7, 2021*. OpenReview.net, 2021. 3

[15] Alexey Dosovitskiy, Lucas Beyer, Alexander Kolesnikov, Dirk Weissenborn, Xiaohua Zhai, Thomas Unterthiner, Mostafa Dehghani, Matthias Minderer, Georg Heigold, Sylvain Gelly, et al. An image is worth 16x16 words: Transformers for image recognition at scale, 2021. 5

[16] Jiafei Duan, Yi Ru Wang, Mohit Shridhar, Dieter Fox, and Ranjay Krishna. Ar2-d2: Training a robot without a robot. In *Conference on Robot Learning*, pages 2838–2848. PMLR, 2023. 2

[17] Jiafei Duan, Wentao Yuan, Wilbert Pumacay, Yi Ru Wang, Kiana Ehsani, Dieter Fox, and Ranjay Krishna. Manipulate-anything: Automating real-world robots using vision-language models. *arXiv preprint arXiv:2406.18915*, 2024.

[18] Hao-Shu Fang, Hongjie Fang, Zhenyu Tang, Jirong Liu, Chenxi Wang, Junbo Wang, Haoyi Zhu, and Cewu Lu. Rh20t: A comprehensive robotic dataset for learning diverse skills in one-shot, 2023. 2

[19] Pete Florence, Corey Lynch, Andy Zeng, Oscar Ramirez, Ayzaan Wahid, Laura Downs, Adrian Wong, Johnny Lee, Igor Mordatch, and Jonathan Tompson. Implicit behavioral cloning, 2021. 3

[20] Yankai Fu, Qiuixuan Feng, Ning Chen, Zichen Zhou, Mengzhen Liu, Mingdong Wu, Tianxing Chen, Shanyu Rong, Jiaming Liu, Hao Dong, et al. Cordvip: Correspondence-based visuomotor policy for dexterous manipulation in real-world. *arXiv preprint arXiv:2502.08449*, 2025. 3

[21] Samir Yitzhak Gadre, Gabriel Ilharco, Alex Fang, Jonathan Hayase, Georgios Smyrnis, Thao Nguyen, Ryan Marten, Mitchell Wortsman, Dhruba Ghosh, Jieyu Zhang, et al. Data-comp: In search of the next generation of multimodal datasets. *Advances in Neural Information Processing Systems*, 36, 2024. 2

[22] Jensen Gao, Annie Xie, Ted Xiao, Chelsea Finn, and Dorsa Sadigh. Efficient data collection for robotic manipulation via compositional generalization, 2024. 2

[23] Ankit Goyal, Jie Xu, Yijie Guo, Valts Blukis, Yu-Wei Chao, and Dieter Fox. Rvt: Robotic view transformer for 3d object manipulation. In *Conference on Robot Learning*, pages 694–710. PMLR, 2023. 6

[24] Raghav Goyal, Samira Ebrahimi Kahou, Vincent Michalski, Joanna Materzynska, Susanne Westphal, Heuna Kim, Valentin Haenel, Ingo Fruend, Peter Yianilos, Moritz Mueller-Freitag, et al. The “something something” video database for learning and evaluating visual common sense. In *Proceedings of the IEEE international conference on computer vision*, pages 5842–5850, 2017. 2

[25] Kristen Grauman, Andrew Westbury, Eugene Byrne, Zachary Chavis, Antonino Furnari, Rohit Girdhar, Jackson Hamburger,

Hao Jiang, Miao Liu, Xingyu Liu, et al. Ego4d: Around the world in 3,000 hours of egocentric video. In *Proceedings of the IEEE/CVF Conference on Computer Vision and Pattern Recognition*, pages 18995–19012, 2022. 2

[26] Kaiming He, Xiangyu Zhang, Shaoqing Ren, and Jian Sun. Deep residual learning for image recognition. In *Proceedings of the IEEE Conference on Computer Vision and Pattern Recognition (CVPR)*, 2016. 3

[27] Kaiming He, Xinlei Chen, Saining Xie, Yanghao Li, Piotr Dollár, and Ross Girshick. Masked autoencoders are scalable vision learners. In *Proceedings of the IEEE/CVF Conference on Computer Vision and Pattern Recognition (CVPR)*, pages 16000–16009, 2022. 3

[28] Kaiming He, Xinlei Chen, Saining Xie, Yanghao Li, Piotr Dollár, and Ross Girshick. Masked autoencoders are scalable vision learners. In *Proceedings of the IEEE/CVF conference on computer vision and pattern recognition*, pages 16000–16009, 2022. 2, 5

[29] Alexander Herzog, Kanishka Rao, Karol Hausman, Yao Lu, Paul Wohlhart, Mengyuan Yan, Jessica Lin, Montserrat Gonzalez Arenas, Ted Xiao, Daniel Kappler, et al. Deep rl at scale: Sorting waste in office buildings with a fleet of mobile manipulators, 2023. 2

[30] Intel Corporation. Intel®realsense™lidar camera l515. <https://www.intelrealsense.com/lidar-camera-1515/>, 2025. Accessed: 2025-02-01. 6

[31] Stephen James, Zicong Ma, David Rovick Arrojo, and Andrew J. Davison. Rlbench: The robot learning benchmark & learning environment. *IEEE Robotics and Automation Letters*, 2020. 5

[32] Eric Jang, Alex Irpan, Mohi Khansari, Daniel Kappler, Frederik Ebert, Corey Lynch, Sergey Levine, and Chelsea Finn. Bc-z: Zero-shot task generalization with robotic imitation learning, 2022. 2

[33] Yueru Jia, Jiaming Liu, Sixiang Chen, Chenyang Gu, Zhilue Wang, Longzan Luo, Lily Lee, Pengwei Wang, Zhongyuan Wang, Renrui Zhang, and Shanghang Zhang. Lift3d foundation policy: Lifting 2d large-scale pretrained models for robust 3d robotic manipulation, 2024. 6

[34] Guangqi Jiang, Yifei Sun, Tao Huang, Huanyu Li, Yongyuan Liang, and Huazhe Xu. Robots pre-train robots: Manipulation-centric robotic representation from large-scale robot datasets, 2024. 5

[35] Dmitry Kalashnikov, Jacob Varley, Yevgen Chebotar, Benjamin Swanson, Rico Jonschkowski, Chelsea Finn, Sergey Levine, and Karol Hausman. Mt-opt: Continuous multi-task robotic reinforcement learning at scale, 2021. 2

[36] Siddharth Karamcheti, Suraj Nair, Annie S. Chen, Thomas Kollar, Chelsea Finn, Dorsa Sadigh, and Percy Liang. Language-driven representation learning for robotics. In *Robotics: Science and Systems (RSS)*, 2023. 2, 3

[37] Simar Kareer, Dhruv Patel, Ryan Punamiya, Pranay Mathur, Shuo Cheng, Chen Wang, Judy Hoffman, and Danfei Xu. Egomimic: Scaling imitation learning via egocentric video, 2024. 3

[38] Alexander Khazatsky, Karl Pertsch, Suraj Nair, Ashwin Balakrishna, Sudeep Dasari, Siddharth Karamcheti, Soroush Nasiriany, Mohan Kumar Srirama, Lawrence Yunliang Chen, Kirsty Ellis, et al. Droid: A large-scale in-the-wild robot manipulation dataset, 2024. 2, 5

[39] Alexander Kirillov, Eric Mintun, Nikhila Ravi, Hanzi Mao, Chloe Rolland, Laura Gustafson, Tete Xiao, Spencer Whitehead, Alexander C. Berg, Wan-Yen Lo, Piotr Dollár, and Ross Girshick. Segment anything, 2023. 2, 4

[40] Alex X Lee, Coline Manon Devin, Yuxiang Zhou, Thomas Lampe, Konstantinos Bousmalis, Jost Tobias Springenberg, Arunkumar Byravan, Abbas Abdolmaleki, Nimrod Gileadi, David Khosid, et al. Beyond pick-and-place: Tackling robotic stacking of diverse shapes, 2021. 2

[41] Sergey Levine, Peter Pastor, Alex Krizhevsky, Julian Ibarz, and Deirdre Quillen. Learning hand-eye coordination for robotic grasping with deep learning and large-scale data collection. *The International Journal of Robotics Research*, 37(4-5):421–436, 2018. 3

[42] Jeffrey Li, Alex Fang, Georgios Smyrnis, Maor Ivgi, Matt Jordan, Samir Yitzhak Gadre, Hritik Bansal, Eshash Guha, Sedrick Scott Keh, Kushal Arora, et al. Datacomp-lm: In search of the next generation of training sets for language models. *Advances in Neural Information Processing Systems*, 37:14200–14282, 2024. 2

[43] Shuang Li, Yihuai Gao, Dorsa Sadigh, and Shuran Song. Unified video action model, 2025. 8

[44] Tsung-Yi Lin, Michael Maire, Serge Belongie, James Hays, Pietro Perona, Deva Ramanan, Piotr Dollár, and C. Lawrence Zitnick. Microsoft coco: Common objects in context. In *Computer Vision – ECCV 2014*, pages 740–755, Cham, 2014. Springer International Publishing. 3

[45] Jianlan Luo, Charles Xu, Jeffrey Wu, and Sergey Levine. Precise and dexterous robotic manipulation via human-in-the-loop reinforcement learning, 2024. 3

[46] Ajay Mandlekar, Danfei Xu, Josiah Wong, Soroush Nasiriany, Chen Wang, Rohun Kulkarni, Li Fei-Fei, Silvio Savarese, Yuke Zhu, and Roberto Martín-Martín. What matters in learning from offline human demonstrations for robot manipulation, 2021. 3, 5

[47] Suraj Nair, Aravind Rajeswaran, Vikash Kumar, Chelsea Finn, and Abhinav Gupta. R3m: A universal visual representation for robot manipulation. *arXiv preprint arXiv:2203.12601*, 2022. 2, 3, 5

[48] Abby O'Neill, Abdul Rehman, Abhiram Maddukuri, Abhishek Gupta, Abhishek Padalkar, Abraham Lee, Acorn Poooley, Agrim Gupta, Ajay Mandlekar, Ajinkya Jain, et al. Open x-embodiment: Robotic learning datasets and rt-x models, 2024. 2, 3

[49] Simone Parisi, Aravind Rajeswaran, Senthil Purushwalkam, and Abhinav Gupta. The unsurprising effectiveness of pre-trained vision models for control. In *Proceedings of the 39th International Conference on Machine Learning*, pages 17359–17371. PMLR, 2022. 3

[50] Georgios Pavlakos, Dandan Shan, Ilija Radosavovic, Angjoo Kanazawa, David Fouhey, and Jitendra Malik. Reconstructing hands in 3d with transformers, 2023. 2, 3

[51] Alec Radford, Jong Wook Kim, Chris Hallacy, Aditya Ramesh, Gabriel Goh, Sandhini Agarwal, Girish Sastry,

Amanda Askell, Pamela Mishkin, Jack Clark, et al. Learning transferable visual models from natural language supervision, 2021. 4

[52] Ilija Radosavovic, Tete Xiao, Stephen James, Pieter Abbeel, Jitendra Malik, and Trevor Darrell. Real-world robot learning with masked visual pre-training, 2022. 3

[53] Ilija Radosavovic, Baifeng Shi, Letian Fu, Ken Goldberg, Trevor Darrell, and Jitendra Malik. Robot learning with sensorimotor pre-training. In *7th Annual Conference on Robot Learning*, 2023. 3

[54] Ilija Radosavovic, Baifeng Shi, Letian Fu, Ken Goldberg, Trevor Darrell, and Jitendra Malik. Robot learning with sensorimotor pre-training. In *Conference on Robot Learning*, pages 683–693. PMLR, 2023. 3

[55] Robotiq Inc. Adaptive grippers. <https://robotiq.com/products/adaptive-grippers>, 2025. Accessed: 2025-02-01. 6

[56] Christoph Schuhmann, Richard Vencu, Romain Beaumont, Robert Kaczmarczyk, Clayton Mullis, Aarush Katta, Theo Coombes, Jenia Jitsev, and Aran Komatsuzaki. Laion-400m: Open dataset of clip-filtered 400 million image-text pairs. *ArXiv*, abs/2111.02114, 2021. 3

[57] Shuai Shao, Zeming Li, Tianyuan Zhang, Chao Peng, Gang Yu, Xiangyu Zhang, Jing Li, and Jian Sun. Objects365: A large-scale, high-quality dataset for object detection. In *2019 IEEE/CVF International Conference on Computer Vision (ICCV)*, pages 8429–8438, 2019. 3

[58] Kenneth Shaw, Ananye Agarwal, and Deepak Pathak. Leap hand: Low-cost, efficient, and anthropomorphic hand for robot learning, 2023. 6

[59] Mohit Shridhar, Lucas Manuelli, and Dieter Fox. Perceiver-actor: A multi-task transformer for robotic manipulation. In *Conference on Robot Learning*, pages 785–799. PMLR, 2023. 6

[60] Roman Suvorov, Elizaveta Logacheva, Anton Mashikhin, Anastasia Remizova, Arsenii Ashukha, Aleksei Silvestrov, Naejin Kong, Harshith Goka, Kiwoong Park, and Victor Lemitsky. Resolution-robust large mask inpainting with fourier convolutions, 2021. 2, 4

[61] Faraz Torabi, Garrett Warnell, and Peter Stone. Behavioral cloning from observation. *arXiv preprint arXiv:1805.01954*, 2018. 3

[62] Tete Xiao, Ilija Radosavovic, Trevor Darrell, and Jitendra Malik. Masked visual pre-training for motor control. *arXiv preprint arXiv:2203.06173*, 2022. 2, 3, 5

[63] Jingyun Yang, Zi ang Cao, Congyue Deng, Rika Antonova, Shuran Song, and Jeannette Bohg. Equibot: Sim(3)-equivariant diffusion policy for generalizable and data efficient learning, 2024. 3

[64] Xumin Yu, Lulu Tang, Yongming Rao, Tiejun Huang, Jie Zhou, and Jiwen Lu. Point-bert: Pre-training 3d point cloud transformers with masked point modeling. In *Proceedings of the IEEE/CVF conference on computer vision and pattern recognition*, pages 19313–19322, 2022. 2

[65] Yanjie Ze, Gu Zhang, Kangning Zhang, Chenyuan Hu, Muhan Wang, and Huazhe Xu. 3d diffusion policy: Generalizable visuomotor policy learning via simple 3d representations. In *Proceedings of Robotics: Science and Systems (RSS)*, 2024. 3

[66] Jia Zeng, Qingwen Bu, Bangjun Wang, Wenke Xia, Li Chen, Hao Dong, Haoming Song, Dong Wang, Di Hu, Ping Luo, Heming Cui, Bin Zhao, Xuelong Li, Yu Qiao, and Hongyang Li. Learning manipulation by predicting interaction, 2024. 2

[67] Jia Zeng, Qingwen Bu, Bangjun Wang, Wenke Xia, Li Chen, Hao Dong, Haoming Song, Dong Wang, Di Hu, Ping Luo, et al. Learning manipulation by predicting interaction. *arXiv preprint arXiv:2406.00439*, 2024. 2

[68] Tony Z Zhao, Vikash Kumar, Sergey Levine, and Chelsea Finn. Learning fine-grained bimanual manipulation with low-cost hardware. *arXiv preprint arXiv:2304.13705*, 2023. 2, 3, 6, 7, 8

H2R: A Human-to-Robot Data Augmentation for Robot Pre-training from Videos

Supplementary Material

A. Details of Simulator Camera Position Alignment

We define two coordinate systems: C_H , the coordinate system aligned with the human hand, and C_S , the coordinate system of the robot arm in the simulator. We build the coordinate system ${}^W\mathbf{I}_H$ based on the hand keypoints:

$${}^W\mathbf{I}_H = \{{}^w\mathbf{i}_{H,x}, {}^w\mathbf{i}_{H,y}, {}^w\mathbf{i}_{H,z}\} \quad (2)$$

Where ${}^w\mathbf{i}_{H,x}, {}^w\mathbf{i}_{H,y}, {}^w\mathbf{i}_{H,z}$ are unit vectors along the x-axes, y-axes and z-axes of the human hand coordinate system. With the keypoints get in HaMeR, we build the three axis of coordinates with the following functions:

$$\begin{aligned} {}^w\mathbf{i}_{H,x} &= {}^w\mathbf{i}_{0,9} \\ {}^w\mathbf{i}_{H,y} &= {}^w\mathbf{i}_{0,9} \times {}^w\mathbf{i}_{0,13} \\ {}^w\mathbf{i}_{H,z} &= {}^w\mathbf{i}_{H,x} \times {}^w\mathbf{i}_{H,y} \end{aligned} \quad (3)$$

Where ${}^w\mathbf{i}_{0,9}$ and ${}^w\mathbf{i}_{0,13}$ are unit vectors along the middle and ring fingers, respectively. In this notation, the first index (0) refers to the specific finger (middle or ring), and the second index (9 and 13) corresponds to the joint numbers along those fingers, as defined by the MANO model. Similarly, To construct the mapping from hand pose to robot arms, we need to get another coordinate system ${}^W\mathbf{I}_S$ in the simulator:

$${}^W\mathbf{I}_S = \{{}^w\mathbf{i}_{S,x}, {}^w\mathbf{i}_{S,y}, {}^w\mathbf{i}_{S,z}\} \quad (4)$$

The method of determining the axis of coordinates is the same:

$$\begin{aligned} {}^w\mathbf{i}_{S,x} &= {}^w\mathbf{i}_{0,2} \\ {}^w\mathbf{i}_{S,y} &= {}^w\mathbf{i}_{0,2} \times {}^w\mathbf{i}_{0,3} \\ {}^w\mathbf{i}_{S,z} &= {}^w\mathbf{i}_{S,x} \times {}^w\mathbf{i}_{S,y} \end{aligned} \quad (5)$$

Where $\mathbf{i}_{0,2}, \mathbf{i}_{0,3}$ are unit vectors along robot fingers that correspond to human middle and ring fingers and the index corresponds to the joint numbers defined by MANO. We build the following two coordinate transformation matrix to construct the mapping:

$$\begin{aligned} {}^H\mathbf{R} &= \begin{pmatrix} {}^W\mathbf{I}_H & \mathbf{key}_{human} \\ \mathbf{O} & 1 \end{pmatrix} \\ {}^S\mathbf{R} &= \begin{pmatrix} {}^W\mathbf{I}_S & \mathbf{key}_{robot} \\ \mathbf{O} & 1 \end{pmatrix} \end{aligned} \quad (6)$$

Where $\mathbf{key}_{human}, \mathbf{key}_{robot}$ are the positions of human wrist and robot wrist. After obtaining the two coordinate systems, we need to determine the position of the camera in the simulator (${}^W\mathbf{cam}_{sim}$) and the position of the camera in

the real world (${}^H\mathbf{cam}_{Real}$), thus we can ensure we get the same pose of the human hand and robot arms

$$\begin{aligned} {}^H\mathbf{cam}_{Real} &= {}^W\mathbf{R}^{-1} \times {}^W\mathbf{cam}_{Real} \\ {}^S\mathbf{cam}_{sim} &= {}^H\mathbf{cam}_{Real} \\ {}^W\mathbf{cam}_{sim} &= {}^S\mathbf{R} \times {}^W\mathbf{R}^{-1} \times {}^W\mathbf{cam}_{Real} \end{aligned} \quad (7)$$

B. Details of Experimental Setup

Data Collection in Real-world Experiment. For the UR5-gripper, demonstration trajectories were collected via keyboard-based teleoperation. For the UR5-Leaphand, demonstrations were gathered using vision-guided teleoperation. For the Dual-arm Franka and Dual-arm UR5 setups, data collection was performed through homogeneous-arm bilateral teleoperation.

Additional Evaluation Details. Figure 7 provides visualizations of the different simulation benchmarks, and Figure 8 illustrates the real-world experimental setup. For the simulation benchmarks, we use the default configurations for both training and evaluation. In the real-world tasks, the UR5-Gripper and UR5-Leaphand setups use the camera shown in Figure 8 as the visual input, whereas the dual-arm Franka and dual-arm UR5 configurations use a front-top camera together with two wrist-mounted cameras (three cameras in total) for visual observation. To ensure that the initial conditions are evaluated consistently across algorithms, we randomly place the target objects within a predefined area following a uniform distribution during expert demonstration collection. During evaluation, the object placement region is kept identical to that used in data collection, ensuring a fair and consistent comparison.

C. Failure Case Analysis

To better understand the limitations of our policy and the challenges encountered in real-world deployments, we present a qualitative analysis of failure cases from two representative tasks: a gripper-based task (*Gripper-Stack*) and a dexterous manipulation task (*Gripper-StandCup*). Figure 9 illustrates typical failure modes observed during execution.

In the **Gripper-Stack** task, we identify two major failure scenarios:

Case I: Grasp Failure Unnoticed. The robot arm fails to successfully grasp the blue cube. However, the policy proceeds as if the object had been grasped, moving toward the yellow cube and attempting to perform the stacking operation. This leads to a complete task failure.

Case II: Misaligned Placement. The robot successfully grasps the blue cube but fails to align it correctly on top of

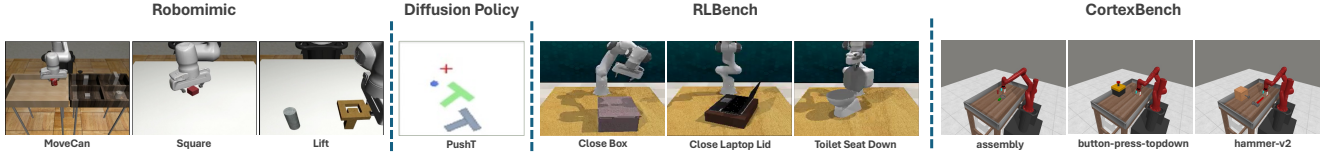


Figure 7. **Simulation benchmark.** We choose 3 tasks from the Robomimic, 3 tasks from the RLBench, and 3 tasks from the CortexBench, covering a range of robotic manipulation skills. We also include the PushT task, designed for the Diffusion Policy framework, as an additional benchmark to evaluate performance in a different task setup.

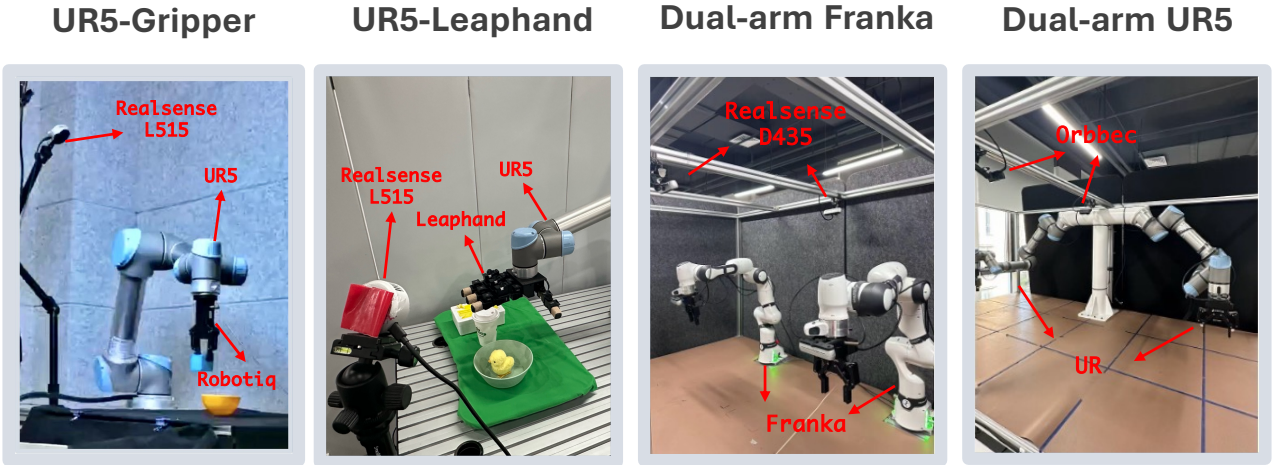


Figure 8. **Real-world Robot Setup.** Illustration of different real-world experimental setup.

the yellow cube during the stacking phase, resulting in an unstable or failed placement.

In the **Stand Cup** task, similar issues emerge due to perception and control limitations:

Case I: Grasp Position Error. The Leaphand end-effector attempts to grasp the cup but fails to target the correct contact region. As a result, the cup slips out of the grasp during lifting, preventing task completion.

Case II: Insufficient Lifting Trajectory. Even when the grasp is successful, the lifting motion lacks sufficient amplitude or stability to fully stand the cup upright. The cup either tips over or fails to stand securely.

To enable fine-grained evaluation of policy performance and gain deeper insights into failure cases, we designed a task-specific evaluation rubric. Table 12 displays our rubric that the evaluator filled out when rolling out different policies. Take the DP policy as an example, the results in Table 12 demonstrate that H2R-augmented visual representation models not only improve overall success rates in real-world tasks, but also allow to accomplish more than half of the task consistently.

D. Additional Ablation Study in Simulation Experiment

In addition to pre-training on the H2R data and raw data, we also applied a simple CutMix baseline to demonstrate the effectiveness of using the robotic arm to cover the human hand, which overlays a fixed set of specific images of robotic arms with grippers onto the original images, ensuring that the overlaid images cover the human hands as much as possible, without exceeding the detected bounding box. Our H2R is different from such baseline by employing robot hand construction to better match the pose of the hand and arm in the images. Based on the type of robotic arm used in CutMix, we categorize the augmented set into three types: CutMix1 represents the UR5 robotic arm, CutMix2 refers to the Franka robotic arm, and CutMix3 combines both the UR5 and Franka robotic arms.

From Table 13, we observe that the encoder trained on H2R processed data shows consistent improvements across various tasks compared to the encoder trained on the original data, with the average success rate on all tasks ranging from 0.9% to 10.2%. Especially for the more challenging MoveCan task, it can improve the success rate by 25.5%. Additionally, while encoders trained on the relatively simple CutMix data show improvement on tasks in Robomimic,

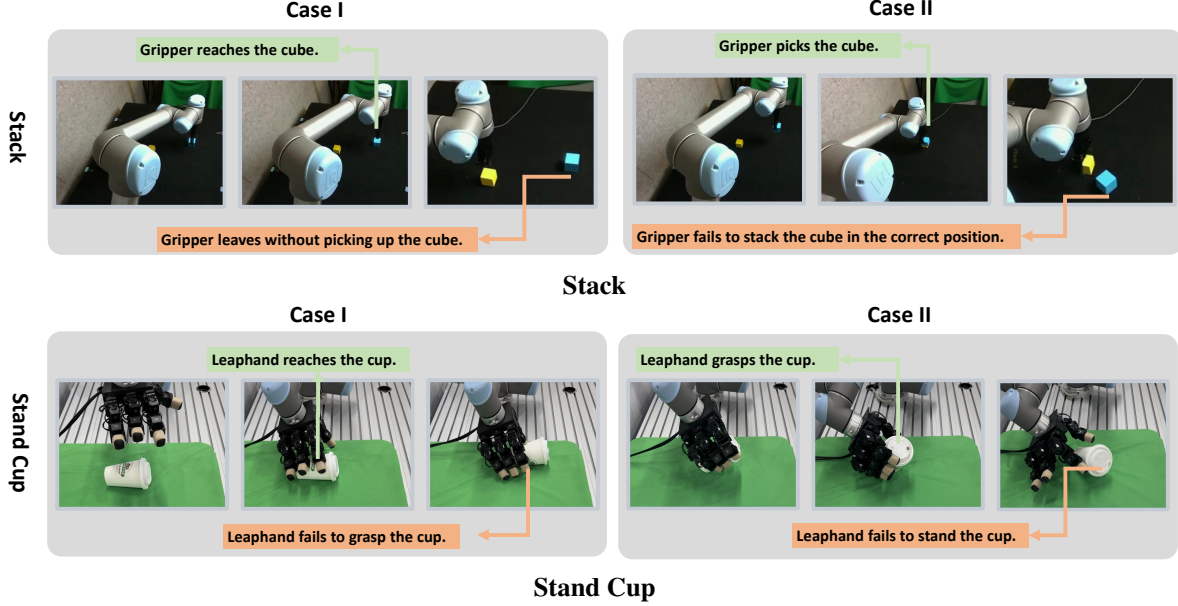


Figure 9. **Failure case visualizations: Stack and Stand Cup.** We visualize real-world manipulation executions for two downstream tasks: **Stack** (top) and **Stand Cup** (bottom). These images provide qualitative insights into the performance and failure modes of the policy in real deployment, highlighting challenges such as object misalignment, perception noise, and grasp precision.

Table 12. **Sub-goal.Task-specific sub-goal evaluation.** To gain fine-grained insights into policy performance, we design a manual rubric covering key sub-goals for each manipulation task. Each cell reports the number of successful vs. unsuccessful attempts (Y/N) over 20 evaluation trials. Results show that models enhanced with H2R consistently accomplish more sub-goals across tasks compared to their baseline counterparts, demonstrating improved robustness in real-world execution. Bold numbers indicate better performance between paired models.

Task	Sub-goal	MAE(Y/N)	MAE+H2R(Y/N)	R3M(Y/N)	R3M+H2R(Y/N)
Gripper-PickCube	Overall success?	9/11	13/7	8/12	10/10
	Pick up the cube?	14/6	15/5	11/9	13/7
Gripper-Stack	Overall success?	10/10	11/9	11/9	14/6
	Pick up the cube?	13/7	16/4	13/7	17/3
Gripper-CloseBox	Overall success?	11/9	10/10	9/11	13/7
	Place the cube in the box?	12/8	14/6	12/8	15/5
	Pick up the cube?	14/6	14/6	12/8	15/5
Leaphand-GraspChicken	Overall success?	8/12	11/9	2/18	7/13
	Pick up the chicken?	13/7	14/6	3/17	10/10
Leaphand-StandCup	Overall success?	7/13	12/8	4/16	10/10
	Pick up the cup?	12/8	18/2	12/8	15/5
Leaphand-OpenBox	Overall success?	9/11	13/7	8/12	9/11
	Identify contact location?	14/6	16/4	10/10	10/10

their performance in the PushT task remains slightly worse than the encoders trained on original data. These results demonstrate the effectiveness of using the robotic arm to cover the human hand in video data, as well as the effectiveness of H2R in imitation learning.

E. Generalization on Light Condition.

To evaluate the generalization under varying lighting conditions, we introduce illumination disturbances during evaluation, as illustrated in Figure 10. Additionally, during training, we incorporate randomized lighting with

Table 13. **Robomimic Experiment result.** We report the success rate (%) over IL-based tasks for MAE and R3M Robomimic.

	MoveCan	Square	Lift	Average		PushT
MAE	54	25.5	94.5	58		59.2
MAE+CutMix1	72.0 (+18.0%)	30.0 (+4.5%)	95.0 (+0.5%)	65.7 (+7.7%)		37.5 (-21.7%)
MAE+CutMix2	58.0 (+4.0%)	36.0 (+10.5%)	90.0 (-4.5%)	61.3 (+3.3%)		40.0 (-19.2%)
MAE+CutMix3	78.0 (+24.0%)	32.0 (+9.3%)	92.0 (-2.5%)	67.3 (+2.7%)		42.0 (-17.2%)
MAE+H2R	79.5 (+25.5%)	29.5 (+4.0%)	95.5 (+1.0%)	68.2 (+10.2%)		64.5 (+5.3%)
R3M	59.5	20.5	85	55		15
R3M+CutMix1	69.5 (+10.0%)	30.0 (+9.5%)	91.0 (+6.0%)	63.5 (+8.5%)		19.0 (+4.0%)
R3M+CutMix2	66.0 (+6.5%)	26.0 (+5.5%)	83.0 (-2.0%)	58.3 (+3.3%)		17.0 (+2.0%)
R3M+CutMix3	68.0 (+8.5%)	26.0 (+5.5%)	84.0 (-1.0%)	59.3 (+4.3%)		14.0 (-1.0%)
R3M+H2R	61.5 (+2.0%)	37.5 (+17.0%)	85.0 (0.0%)	61.3 (+6.3%)		22.0 (+7.0%)

Table 14. **Generalization under Lighting Variations.** Success rates (%) under real-world lighting disturbances. Models trained with additional lighting augmentations (LightAug) show significant improvements in robustness compared to baseline and H2R-only models.

Tasks	MAE	MAE+H2R	MAE+H2R+LightAug	R3M	R3M+H2R	R3M+H2R+LightAug
LeapHand-GraspChicken	10	10	20	0	0	10
LeapHand-StandCup	20	25	40	5	15	20
LeapHand-OpenBox	5	0	25	10	10	10
Average	11.7	11.7	28.3	5	8.3	13.3

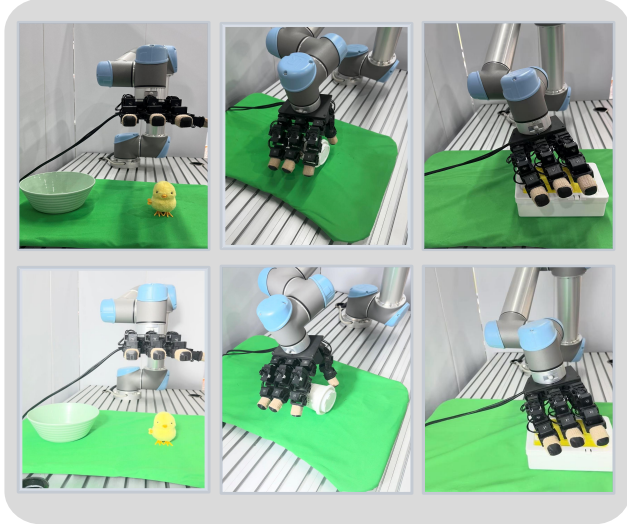


Figure 10. **Lighting Setup in Real-World Experiments.** Light configuration used in real-world evaluations.

highlighting the effectiveness of H2R in bridging the domain gap caused by lighting variations.

varying directions and colors into the simulation environment for data augmentation. We compare three settings: no augmentation(MAE, R3M), H2R augmentation(MAE+H2R, R3M+H2R), and H2R with lighting disturbances(MAE+H2R+LightAug, R3M+H2R+LightAug). As shown in Table 14, the model trained with H2R and lighting perturbations demonstrates significantly better generalization to real-world lighting variations than other baselines,